

# Development of tRNA-based biomarkers for breast cancer: Insight from machine learning

---

## Keywords

prognosis, breast cancer, immunotherapy, tRNA, Machine learning, pan-cancer analysis

---

## Abstract

### Introduction

Breast cancer (BC) is one of the most frequent cancers in women globally. Research on tRNA-related biomarkers for predicting BC survival remains notably lacking. In this study, bioinformatics analysis was utilized to identify tRNA-related gene targets.

### Material and methods

We obtained closely related mRNAs by screening BC prognosis-associated tRNAs from the OncotRF database. Next, we selected prognostically important mRNAs further using the Bruta algorithm. We developed a risk model based on these significant genes by using a variety of machine learning techniques and validated the expression with experiment. Data from the TCGA, GEO, and IMvigor210 datasets were used to validate the predictive efficacy of the t-mRNA characteristics. We also obtained the single-cell RNA sequencing (scRNA-Seq) data from the TISCH2 database and the RNA-Seq data from the UCSC Xena database for pan-cancer analysis.

### Results

We created a prognostic model with 12 t-mRNAs associated with BC. Strong predictive performance of this model was demonstrated by nomogram, ROC and survival analyses. Functional enrichment analysis revealed differences between the low-risk and high-risk groups in immunological-related biological processes. The high-risk group showed reduced immunotherapy efficiency and greater M2 macrophage infiltration, according to the analysis of immune infiltration and immunotherapy responsiveness. Furthermore, the pan-cancer investigation revealed that high-risk tumors typically exhibit more aggressive features. We also found the express difference of model genes between normal and cancer cells.

### Conclusions

We created an t-mRNA feature that may accurately predict the prognosis of BC patients and promote the development of precision medicine for cancer.

# Development of tRNA-based biomarkers for breast cancer: Insight from machine learning

Quan Yuan<sup>a†</sup>, Rongjie Ye<sup>b†</sup>, Hao Yu<sup>c</sup>, Ge Yu<sup>a\*</sup>, Ming Niu<sup>a\*</sup>

a. Harbin Medical University Cancer Hospital, Harbin, China 150040.

b. Fujian Medical University Affiliated First Quanzhou Hospital, Quanzhou, Fujian, China 362000.

c. The First Affiliated Hospital of Xiamen University, School of Medicine, Xiamen University, Xiamen 361000, Fujian, China.

## \* Correspondence:

Ge Yu

[yuhuren@163.com](mailto:yuhuren@163.com)

Ming Niu

[niuming2024@126.com](mailto:niuming2024@126.com)

†Q Y and RJ Ye contributed equally to this paper.

## Abstract

**Introduction:** Breast cancer (BC) is one of the most frequent cancers in women globally. Research on tRNA-related biomarkers for predicting BC survival remains notably lacking. In this study, bioinformatics analysis was utilized to identify tRNA-related gene targets.

**Material and methods:** We obtained closely related mRNAs by screening BC prognosis-associated tRNAs from the OncotRF database. Next, we selected prognostically important mRNAs further using the Bruta algorithm. We developed a risk model based on these significant genes by using a variety of machine learning techniques **and validated the expression with experiment**. Data from the TCGA, GEO, and IMvigor210 datasets were used to validate the predictive efficacy of the t-mRNA characteristics. We also obtained the single-cell RNA sequencing (scRNA-Seq) data from the TISCH2 database and the RNA-Seq data from the UCSC Xena database for pan-cancer analysis.

**Results:** We created a prognostic model with 12 t-mRNAs associated with BC. Strong predictive performance of this model was demonstrated by nomogram, ROC and survival analyses. Functional enrichment analysis revealed differences between the low-risk and high-risk groups in immunological-related biological processes. The high-risk group showed reduced immunotherapy efficiency and greater M2 macrophage infiltration, according to the analysis of immune infiltration and immunotherapy responsiveness. Furthermore, the pan-cancer investigation revealed that high-risk tumors typically exhibit more aggressive features. **We also found the express difference of model genes between normal and cancer cells.**

**Conclusions:** We created an t-mRNA feature that may accurately predict the prognosis of BC patients and promote the development of precision medicine for cancer.

**Keywords:** Machine learning, tRNA, breast cancer, prognosis, immunotherapy, pan-cancer analysis

## 1.Introduction

One of the most common malignant tumors that affect women worldwide, breast cancer (BC) has a major influence on life and health[1]. The US is likely to see 310,720 new female BC cases in 2023, with 42,250 deaths anticipated, according to the

American Cancer Society (ACS)[2]. For early-stage BC, the 5-year survival rate has significantly increased[3]. Less than 30% of patients with metastatic breast cancer survive, however, due to the intrinsic heterogeneity of the tumor, which frequently causes treatment resistance, post-surgical recurrence, and distant metastasis[4], This results in a survival rate of less than 30% for patients with metastatic breast cancer[5]. Therefore, enhancing clinical outcomes depends heavily on comprehending the molecular pathways behind the onset and progress of breast cancer as well as discovering novel biomarkers[6, 7].

We have recently investigated the molecular pathways connected to the development of tumors, paying particular attention to the interaction between transfer RNA (tRNA) and messenger RNA (mRNA). Due to its involvement in the initiation and advance of tumors, this relationship is receiving more attention[8, 9]. A hallmark of tumors is aberrant cell proliferation, which is mostly controlled by protein translation pathways. mRNA and tRNA are important players in gene expression[10]. By matching mRNA codons and contributing particular amino acids to the expanding polypeptide chain at the ribosome, tRNA, a subclass of short non-coding RNA (sncRNA), stimulates the synthesis of proteins[11]. Beyond its conventional function in translation, recent research has highlighted that tRNAs in tumor cells can influence mRNA in various ways to regulate protein translation, thereby impacting tumor biological characteristics[12, 13]. Tumor invasion and aberrant proliferation can be encouraged by changes in tRNAs, which can change the rates at which mRNAs are translated[14, 15]. For example, Ma et al. showed that m7G-modified tRNA could enhance the translation of target mRNAs through a codon frequency-dependent mechanism, encouraging lung cancer cell proliferation, invasion, migration, and colony formation—a factor linked to a poor prognosis for patients with lung cancer[16]. Additionally, tRNA-derived microRNAs (miRNAs) act by suppressing the expression of protein-coding genes through sequence complementarity with mRNA[17]. In summary, tRNA influences cancer progression not only through genomic alterations but also by modifying the malignant phenotype of tumors through changes in mRNA. Research on the function of t-mRNAs related with BC prognosis in the onset and advance of breast cancer is still lacking, despite recent discoveries connecting tRNAs with BC prognosis[14], there remains a lack of research on the role of BC prognosis-associated t-mRNAs in the development and progression of breast cancer.

Machine learning, a significant branch of artificial intelligence in the era of big data, excels at identifying relevant features from large, high-dimensional datasets derived from sequencing studies[18] and is increasingly employed to construct tumor prognosis models[19, 20]. Recognizing the promising prognostic value of tRNA across

various tumors[21, 22], our research utilized ten machine learning methods to generate 101 combinations of machine learning algorithms to identify the t-mRNAs linked with BC prognosis and developed a prognostic model.

Single-cell sequencing enables us to analyze gene expression, mutations, and epigenetic modifications within tumors at the cellular level, shedding light on tumor heterogeneity and the complexity of tumor cell evolution. However, in practice, scRNA-Seq is mostly confined to studying individual cancer types. By integrating single-cell sequencing with pan-cancer analysis, we can uncover potential common driver genes across different cancers and identify subpopulations with similar gene expression profiles, deepening our understanding of cancer development mechanisms. In our study, we also tested the model's efficacy in different cancers, achieving favorable outcomes.

## **2. Materials and methods**

### **2.1 Gathering and processing public data**

We obtained target tRNAs associated with the prognosis of BC from the OncotRF database (<http://bioinformatics.zju.edu.cn/OncotRF>). We downloaded the GSE20711 and GSE20685 from the Gene Expression Omnibus (GEO) database (<https://www.ncbi.nlm.nih.gov/geo/>), which including the expression profiles of 92 and 327 breast cancer patients' tumor and normal tissues. For the purpose of developing and validating our risk model, we accessed data on BC patients from TCGA-BRCA, including 64 patients with metastases and 19 patients with original tumors, from The Cancer Genome Atlas (TCGA) database (<https://tcga-data.nci.nih.gov/tcga/>). In order to investigate potential relationships between t-mRPM and its model genes across various cancers, we also obtained the processed RNA-Seq data of 32 solid malignant tumor types from the UCSC Xena database (<https://xena.ucsc.edu/>). For an extensive pan-cancer analysis, the 32 processed scRNA-Seq datasets and annotations of 32 solid malignant tumor types were additionally acquired from the TISCH2 database (<http://tisch.comp-genomics.org>). The TISCH2 database has already carried out quality control, normalization, unsupervised clustering, and cell type annotation for these datasets.

### **2.2 Screening and functional analysis of t-mRNA related to BC prognosis**

Using the OncotRF database, we screened tRNAs differentiating breast cancer from normal tissues that influence prognosis, selecting from 3'-tRF and 5'-tRF sequences. We calculated Spearman correlation coefficients between these tRNAs and mRNA

expression profiles, defining t-mRNAs as those with a correlation coefficient  $> 0.4$  and  $p < 0.01$ , which were then visualized using Cytoscape[23]. We used Kyoto Encyclopedia of Genes and Genomes (KEGG) pathway analysis to comprehend the biological roles of these mRNAs[24].

### **2.3 Identification of differentially expressed t-mRNA related to BC prognosis**

We first screened prognosis-related genes from t-mRNAs using the Boruta algorithm[25], a random forest-based method for feature ranking and selection, to screen prognosis-related genes from t-mRNAs. Next, we examined the mRNA expression matrix between BC samples and normal breast samples using the "limma" package[26]. A false discovery rate (FDR)  $< 0.05$  and an absolute  $\log_2$  (fold change)  $> 1$  were the requirements assigned for finding DE mRNAs. From these results, we obtained BC-related genes and the selected t-mRNA genes. By intersecting these genes, we acquired DE t-mRNAs for further analysis.

### **2.4 Construct t-mRPM using machine learning-based integrative approaches.**

Ten machine learning algorithms and their 101 combinations were applied to guarantee great accuracy and stability of our t-mRPM. Among them were the following: supervised principal components (SuperPC), generalized boosted regression modeling (GBM), random survival forest (RSF), elastic net (Enet), Lasso, Ridge, stepwise Cox, CoxBoost, and survival support vector machine (survival-SVM). Based on the highest average concordance index (C-index), the best model was chosen. We used three datasets (TCGA-BRCA, GSE20711, and GSE20685) for Kaplan-Meier analysis in order to verify the stability and reproducibility of the model. The results were displayed using survival curves. Additionally, we plotted the model's 1-year, 3-year, 5-year, 7-year, and 9-year ROC curves to evaluate the predictive performance.

### **2.5 Association of clinical-pathological features and the construction and validation of nomogram**

**We** examined the relationship between the risk model and pathological features in order to assess the clinical value of t-mRNA. Additionally, we analysis the gene expression patterns across several pathological features in the risk model, which were shown in a heatmap. Furthermore, the TCGA BC metastasis database was used to evaluate the predictive potential for metastasis of BC patients s. The model was then integrated with clinical-pathological variables to produce the nomogram, and calibration and decision curves were used to assess the nomogram's clinical efficacy.

## **2.6 Gene Set Variation Analysis (GSVA) and Single-sample Gene Set Enrichment Analysis (ssGSEA)**

The R package "GSVA"[27] was utilized in our investigation to calculate scores for fifty HALLMARK pathways. The "limma" program was then used to examine pathways that showed notable variations between high- and low-risk groups. In order to determine the contribution of tumor related molecular mechanisms in different risk groups, we used the R package "clusterProfiler"[28] to perform a GSEA analysis of HALLMARK gene sets with  $FDR < 0.25$  and  $|NES| > 1$ .

## **2.7 Immune feature correlation analysis**

Using ssGSEA, we evaluated the variations in immune-related pathways between the groups[29]. The CIBERSORT and xCell algorithms[30] were utilized to quantify the relative abundance of Tumor-Infiltrating Immune Cells (TIICs) within tumor samples. Consideration of recent advances in immunotherapy for BC[31], we utilized the IMgor210 dataset to predict the effects of immunotherapy in BC patients using our model.

## **2.8 Performance of the risk model and its genes in pan-cancer**

We sought to further assess the performance of the model and its genes regarding expression, mutations, copy number variations, and methylation across various cancers. Additionally, we examined the impact of the t-mRPM on the prognosis of different cancers, affirming the model's broad applicability across various tumor types. We also assessed the relationship between the model and features of tumor malignancy such as the cell cycle, angiogenesis, and EMT.

## **2.9 Expression of model genes at the pan-cancer single-cell level**

We obtained single-cell gene expression information from the [TISCH2](#) database, which was used to investigate the relationship between the tumor microenvironment and t-mRNA by examining the single-cell expression of model genes in 32 distinct solid malignant cancer types.

## **2.10 Quantitative real-time PCR (RT-qPCR)**

Human mammary epithelial cells (HS578BST) and breast cancer cell lines (MDA-MB-231 and MCF-7) were procured from Fenghui Biotechnology Co., Ltd. (Hunan, China). These cells were maintained in DMEM medium supplemented with 10% fetal

bovine serum (Gibco) and incubated at 37°C with 5% CO<sub>2</sub>. Total RNA was isolated from cultured cells using TRIzol reagent (Tiangen, Beijing, China) according to the manufacturer's protocol. Then the total RNA was reverse-transcribed into cDNA using RevertAid Reverse Transcriptase (Thermo Fisher Scientific, Waltham, MA, USA). The RT-qPCR analysis was subsequently carried out on the ABI QuantStudio 1 Plus instrument using PerfectStart® Green qPCR SuperMix. The reaction conditions were as follows: initial denaturation at 94 °C for 35 s, annealing at 60 °C for 15 s, and extension at 72 °C for 10 s. Relative gene expression levels were quantified using the 2<sup>-ΔΔCt</sup> method. The primers used in this study were designed by Pulateze Biotech (Hunan, China), as listed in **Table 1**.

## 2.11 Analytical statistics

R software (version 4.1.1) was used for the analysis. Pearson's chi-squared test was utilized to assess categorical data, and one-way ANOVA was employed to investigate continuous variables. A p-value of less than 0.05 was considered statistically significant. The OS of individuals with breast cancer was examined using the Kaplan–Meier method. Cox regression models, both univariate and multivariate, were used to find independent predictive markers and clinical features that varied significantly between patient groups. Using the Mann-Whitney U test, differences in immune cell infiltration were evaluated. Statistical significance was defined as p-values < 0.05 (\*p < 0.05, \*\*p < 0.01, \*\*\*p < 0.001, ns: not significant).

## 3. Result

### 3.1 Identification of the DEt-mRNA

Using the OncotRF database, we first chose a prognostically significant tRNA (5'-M-tRNA-Tyr-GTA-7-1\_L23) in BC. We next calculated the Spearman correlation coefficient to find 92 mRNAs that were substantially related with this tRNA (**Figure 1A**). Meanwhile, we also found these t-mRNAs are mainly involved in pathways that include the cell cycle, the infection of the human T-cell leukemia virus, the p53 signaling pathway, the maturation of oocytes through progesterone, meiosis of oocytes, cellular senescence, leukocyte transendothelial migration, the FoxO signaling pathway (**Figure 1B**). We have identified 62 genes associated with BC prognosis using the Boruta method (**Figures 1C, D**). In TCGA-BRCA cohorts, we found 296 differentially expressed mRNAs (DE-mRNAs), which were visualized on volcano plot (**Figure 1E**). Notably upregulated genes in this plot include MMP11, COL10A1, COMP, COL11A1, and S100P. In the end, these 62 prognostic genes were intersected with the DE-mRNAs

using a Venn diagram (**Figure 1F**), yielding 22 **key** genes that were designated as DEt-mRNAs.

| Primer name     | Primer sequence ( 5'→3') |
|-----------------|--------------------------|
| h-MELK-169-F    | TATTCACCTCGATGATGATTGCG  |
| h-MELK-169-R    | AGAAAGCCTTAAACGAACTGGTT  |
| h-CENPF-102-F   | CTCTCCCGTCAACAGCGTTC     |
| h-CENPF-102-R   | GTTGTGCATATTCTTGGCTTGC   |
| h-TSPAN7-242-F  | TATCTCCCTTATTGCCGAGAACT  |
| h-TSPAN7-242-R  | TAGCGTCCGTGTAAGTCCTCA    |
| h-BIRC5-118-F   | AGGACCACCGCATCTCTACAT    |
| h-BIRC5-118-R   | AAGTCTGGCTCGTTCTCAGTG    |
| h-NEK2-233-F    | CTGGATGGCAAGCAAACGTC     |
| h-NEK2-233-R    | CCAGCGAGTTCTTTCTGGCTA    |
| h-TOP2A-129-F   | ACCATTGCAGCCTGTAAATGA    |
| h-TOP2A-129-R   | GGGCGGAGCAAATATGTTCC     |
| h-GPIHBP1-194-F | GCAACCTGACGCAGAACTG      |
| h-GPIHBP1-194-R | CCAGGGTGGGACATTGCAC      |
| h-COX7A1-132-F  | GAGTGCGCGAGAAACAGAAG     |
| h-COX7A1-132-R  | ACAAGCTGTAGACAGTGCCG     |
| h-SCN4B-179-F   | CTGGGCTTTTGGTGGGAAGAAG   |
| h-SCN4B-179-R   | GTTGTCATTCCCCGAGGAGC     |
| h-ANLN-130-F    | TGGAGAAGAGCCAAGAGGAG     |
| h-ANLN-130-R    | TCTGGACTTACCACACCAACTG   |
| h-UBE2T-226-F   | AGCTGCTCATGTCAGAACCC     |
| h-UBE2T-226-R   | ACTAGCTGACTGGCCTTCCT     |
| h-KIF4A-139-F   | ACGCCATCTGAATGACCTCC     |
| h-KIF4A-139-R   | ACCACGCACTTCAGTAAGGG     |
| hGAPDH-172-F    | CTGACTTCAACAGCGACACC     |
| hGAPDH-172-R    | GTGGTCCAGGGGTCTTACTC     |

**Table 1.** RT-qPCR primer sequences used in the study.

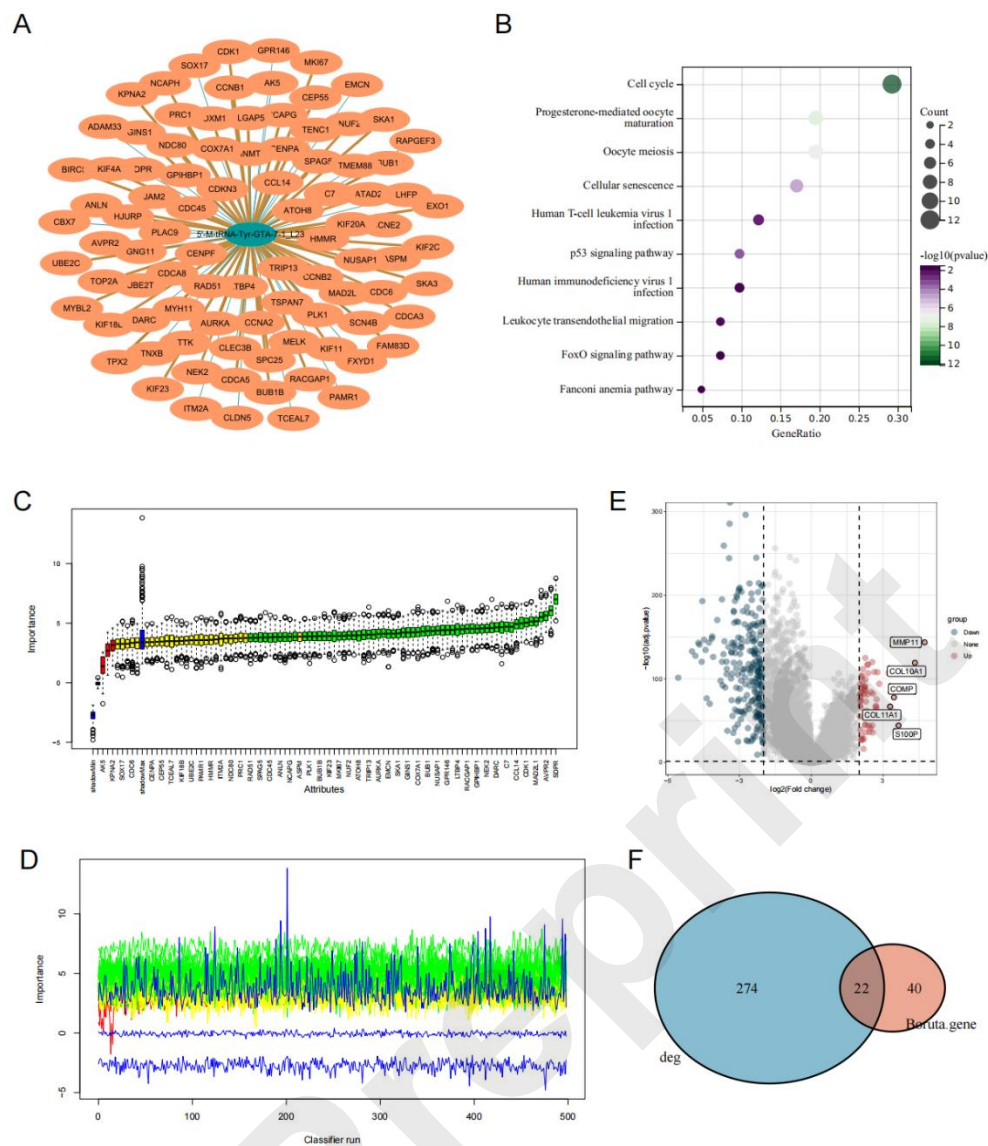


**Figure 1.** Identification of DEt-mRNA. (A) t-mRNA Related Network Diagram. (B) Biological Process Involvement by t-mRNA. (C) t-mRNAs Related to BC Prognosis: Identified by the Boruta algorithm. (D) Feature Selection Detail Diagram: Shows t-

mRNAs selected by the Boruta algorithm across different iterations. (E) Volcano Plot: Displays DE mRNAs between normal and tumor tissues in BC patients. (F) Venn Diagram: Used to identify common genes between DEGs and t-mRNA in BC.

### 3.2 The construction and validation of t-mRPM

An integrative technique based on machine learning was used to the 22 DE t-mRNAs in order to generate a consensus tRNA-related mRNA signature. Even though Ridge had the greatest average C-index (0.616), we decided that the Lasso and CoxBoost combo was the best algorithm pair. This combination achieved the greatest average C-index of 0.611 among all combinations that incorporated Lasso, which affected the decision. Additionally, the combination was required to obtain coefficient values from Lasso regression for a subsequent pan-cancer study (**Figure 2A**). According to the LOOCV framework (**Figure 2B**), the optimal  $\lambda$  for the Lasso regression was found at the point where the partial likelihood deviance was lowest. A definite collection of 12 t-mRNAs was identified by applying CoxBoost proportional hazards regression analysis to t-mRNAs with nonzero Lasso coefficients. These t-mRNAs are MELK, CENPF, TSPAN7, BIRC5, NEK2, TOP2A, GPIHBP1, COX7A1, SCN4B, ANLN, UBE2T, and KIF4A (**Figure 2C**). Next, the expression levels of these 12 t-mRNAs, weighted by their regression coefficients in the CoxBoost model, were used to calculate the risk score for each BC patient, referred to as the t-mRPM score. The 'survminer' R package was implemented to determine the optimal cutoff value, classifying BC patients into high-risk and low-risk groups. As demonstrated in the TCGA training dataset and the GSE20585 validation set, overall survival was significantly lower in the high-risk group compared to the low-risk group ( $p < 0.05$ ) (**Figure 2D-F**). However, in the GSE20711 validation set, there was no significant difference in survival rates between the high and low-risk groups ( $p = 0.21$ ), likely due to the smaller sample size of this validation cohort. ROC analysis assessed the discrimination capability of t-mRPM, with 1-, 3-, 5-, 7-, and 9-year AUC values of 0.72, 0.66, 0.66, 0.66, and 0.63 respectively in TCGA-BRCA, indicating the model's effective predictive power for the OS of BC patients across these time points (**Figure 2G**).

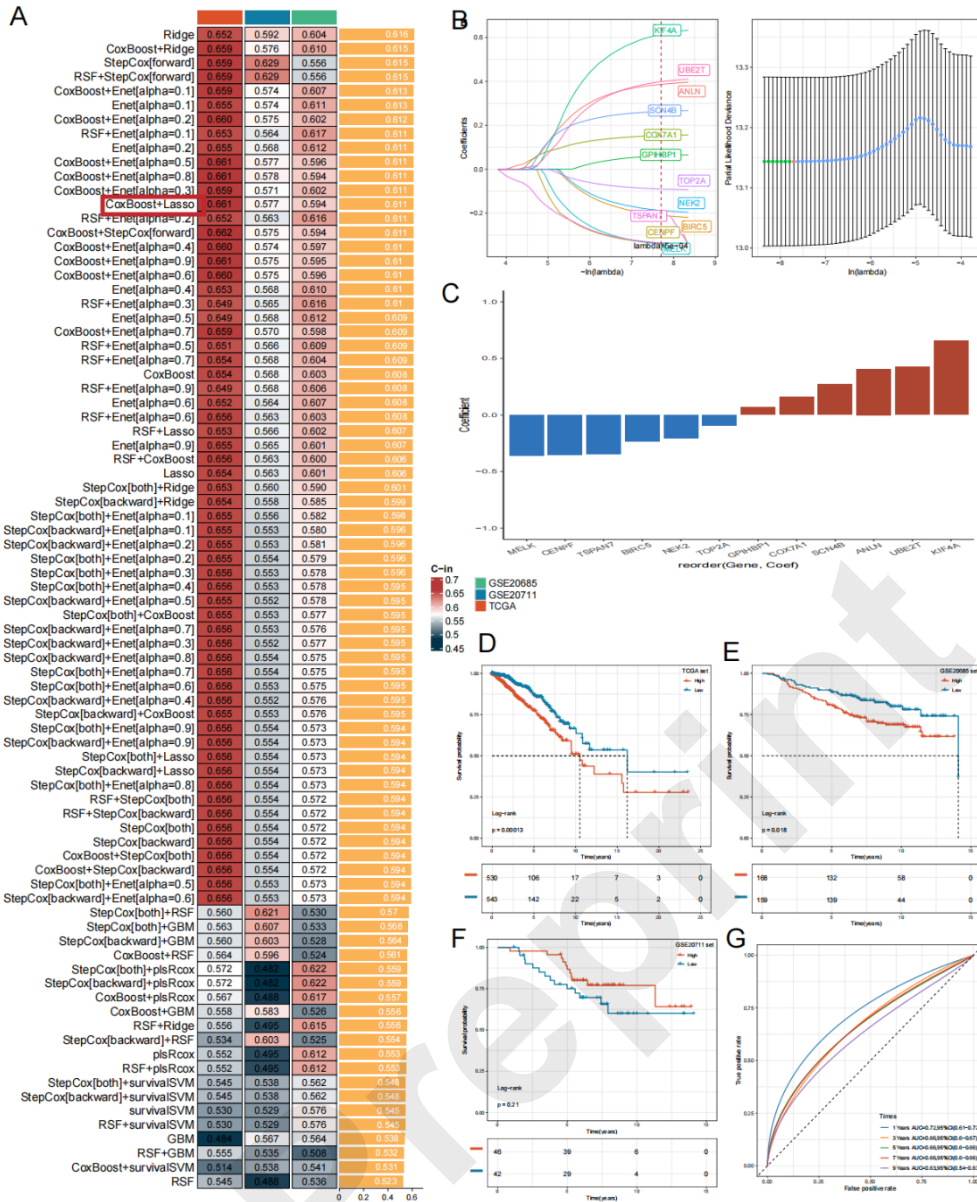


**Figure 2.** Construction and validation of t-mRPM. (A) Created 101 different kinds of prediction models using the LOOCV framework. (B) A logarithmic sequence graph ( $\lambda$ ) that illustrates the t-mRNA by LASSO regression analysis. (C) CoxBoost

regression coefficients for the last set of 12 t-mRNAs. (D-F) Kaplan-Meier curves for OS based on t-mRPM in several datasets. (G) The optimal model's ROC curves.

### 3.3 The correlation between t-mRPM score and clinical-pathological

The TCGA dataset's analysis of the relationship between t-mRPM risk scores and clinical-pathological features showed significant differences ( $p$ -value  $< 0.05$ ) in TNM staging, pathological grading, Fustat, and gender between the high- and low-risk groups (**Figures 3A–B**). As seen in **Figure 3C**, Kaplan-Meier curve analysis indicated that the high-risk group had a worse prognosis than the low-risk group (Log-rank test,  $p < 0.01$ ). Since early BC (stages I and II) still accounts for a significant portion of diagnoses, we first looked at how this risk model varied across different T stages. Patients in later stages (T3-4) showed greater risk ratings than those in early stages (T1-2) (**Figure 3D**;  $p < 0.01$ , Wilcox test). Furthermore, ROC curve analysis showed that the AUC value for t-mRNA predicting M staging was 0.668 (**Figure 3E**), suggesting that the t-mRPM score might also predict the development of distant organ metastasis in BC patients. t-mRPM was also found to be predictive of M staging (M0 and M1). We investigated the predictive power of model genes for BC metastasis using the TCGA-BRCA dataset. While individual genes were not very predictive, the risk model that **consist of** these genes showed better predictive power in predicting metastases of breast cancer ( $p = 0.032$ ) (**Figure 4**). According to this model, metastasis is more likely to occur in patients with higher scores. All things considered, the t-mRPM score enhances the prognosis for BC survival and is a useful predictor of cancer metastasis.

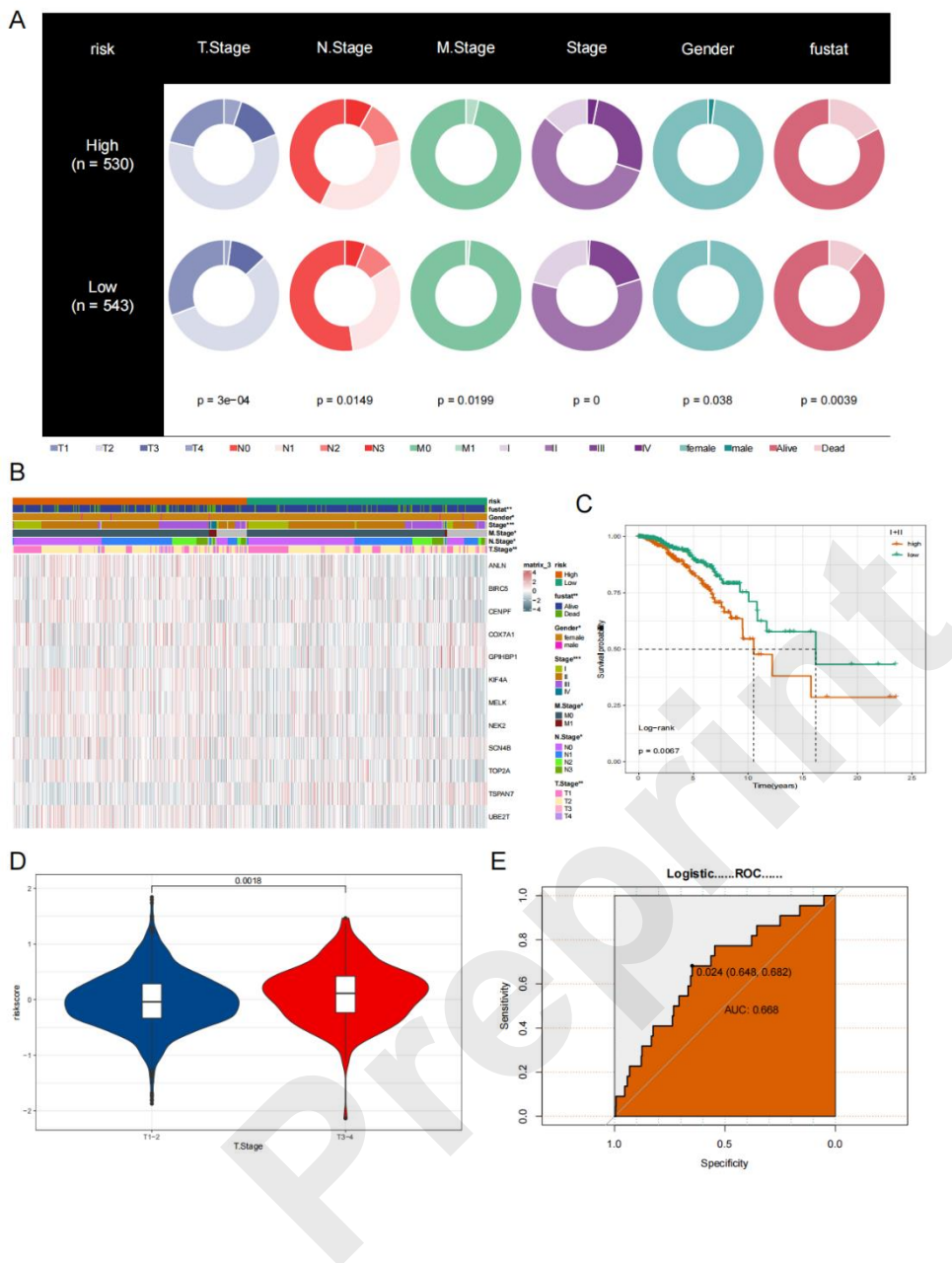


**Figure 3.** Analysis of correlations between various clinicopathological features and the prognostic model in the TCGA cohort. (A) Pie chart showing the relationship between clinical-pathological traits and high- and low-risk groups. (B) A heatmap showing how six distinct clinicopathological traits are distributed along with each patient's risk score determined by their signature. (C) Kaplan-Meier OS curves for breast cancer in its

early stages based on t-mRPM (log-rank test:  $p = 0.0067$ ). (D) Risk scores were considerably greater in patients in stages T3–4 than in those in stages T1-2 ( $p = 0.0018$ ). (E) ROC curves for BC patients showing the M stage prediction (M0 and M1,  $AUC = 0.668$ ).

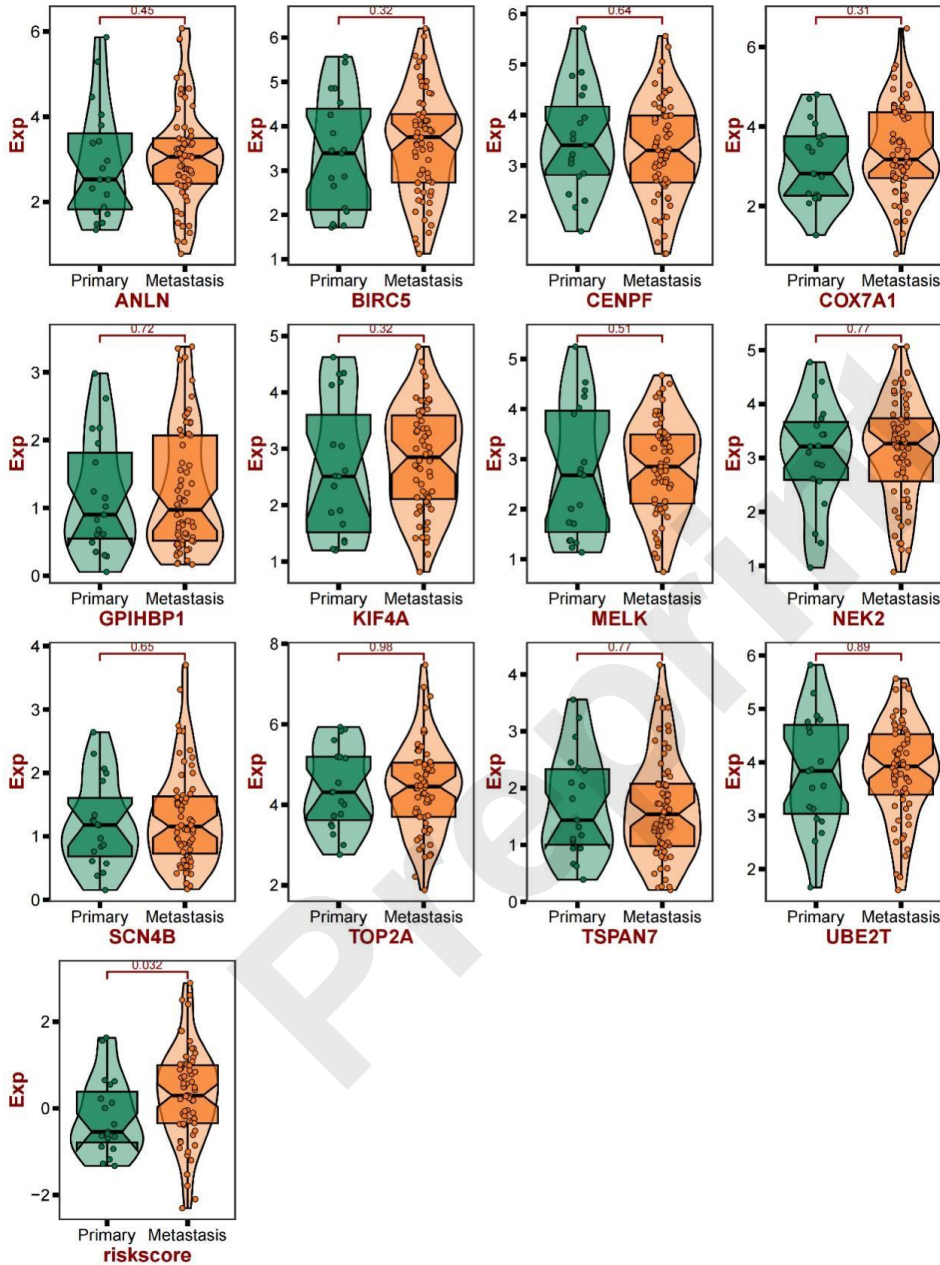


**Figure 4.** Expression levels of individual model genes in the BC metastasis cohort. Green represents the non-metastasis group (primary) and orange represents the metastasis group (Metastasis).

### 3.4 Development and evaluation of nomogram

To confirm the independent predictive capability of t-mRPM, both univariate and multivariate Cox regression analyses were conducted (**Figures 5A-B**). In the univariate analysis, except for gender (HR = 0.815, 95% CI = 0.114-5.836,  $p = 0.839$ ), the clinical-pathological characteristics such as age, TNM staging, pathological staging, and risk score were significantly correlated with prognosis, each indicating a poor prognosis (all  $p < 0.05$ ). These included age (HR = 1.034, 95% CI = 1.02–1.047,  $p < 0.001$ ), T stage (HR = 1.763, 95% CI = 1.225-2.538,  $p = 0.02$ ), M stage (HR = 5.649, 95% CI = 3.387-9.423,  $p < 0.001$ ), N stage (HR = 2.189, 95% CI = 1.533-3.127,  $p < 0.001$ ), overall Stage (HR = 2.628, 95% CI = 1.878-3.678,  $p < 0.001$ ), and Risk score (HR = 2.576, 95% CI = 1.887-3.517,  $p < 0.001$ ) (**Figure 5A**). In the multivariate analysis, the risk score (HR = 2.531, 95% CI = 1.802-3.556,  $P < 0.001$ ) and M stage (HR = 3.541, 95% CI = 1.883-6.659,  $P < 0.001$ ) emerged as independent prognostic factors for predicting adverse OS in BC patients (**Figure 5B**). A predictive nomogram including clinical-pathological variables was developed to predict an individual's overall survival at 1, 3, and 5 years in order to enhance clinical decision-making. This nomogram closely matched the optimal prediction model (**Figures 5C-D**), demonstrating high accuracy in predicting 1-year, 3-year, and 5-year OS. The decision curve analysis (DCA) (**Figure 5E**) and calibration chart (**Figure 5D**) demonstrated that t-mRNA is a reliable prognostic indicator for BC patients, confirming the nomogram's accuracy in predicting survival probability with real outcomes. This enhances predictive models and facilitates clinical judgment.

To explore the difference of biological functions in two risk groups and the research value of model genes in multiple cancer types, we conducted pathway enrichment analysis, immune correlation analysis, and pan-cancer analysis, as detailed in the supplementary materials.

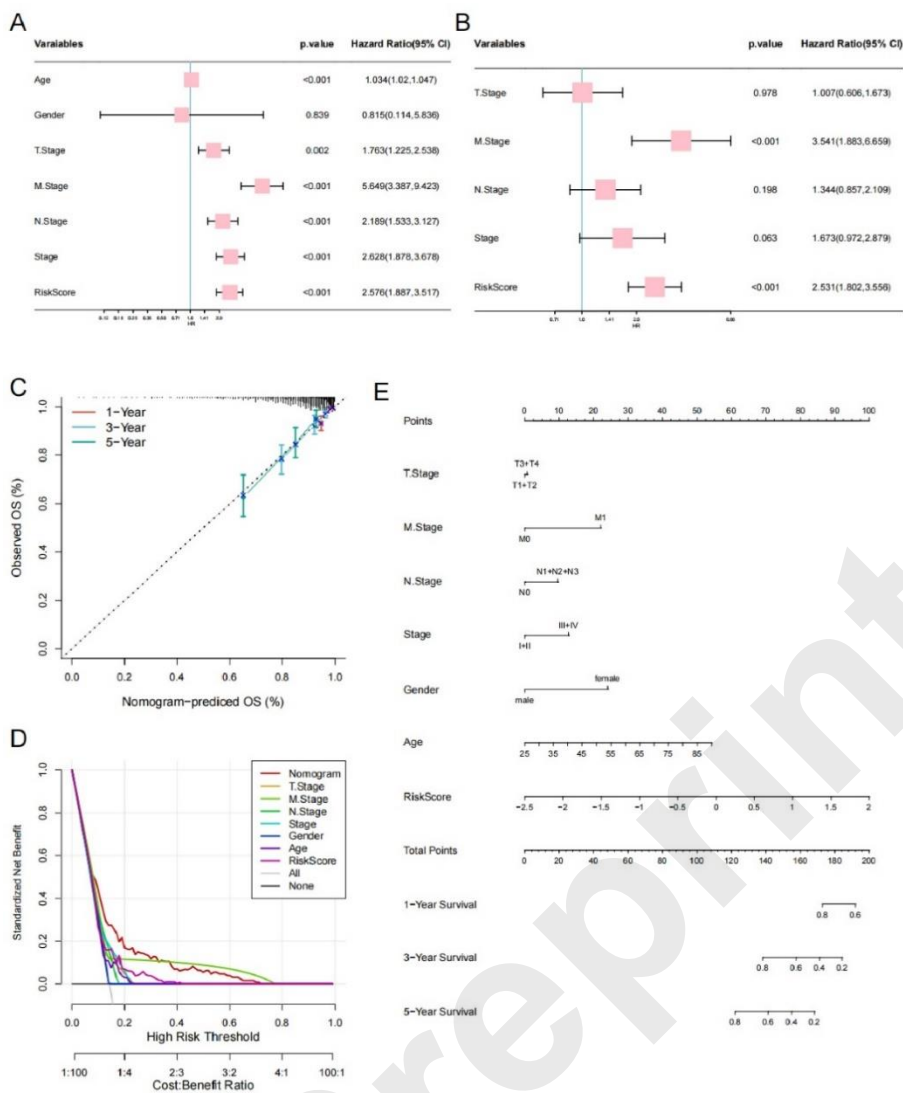


**Figure 5.** Analysis of the clinical pathological characteristics of t-mRPM and its independent prognostic potential. (A–B) The outcomes of the univariate and multivariate Cox regression analyses. (C) A nomogram that can be used to forecast a patient's overall survival. (D) The nomogram's decision curve values. (E) The nomogram model calibration curve.

### 3.5 Validation of the 12 model genes with RT-qPCR assay

To delineate differential expression patterns of model genes between malignant and normal mammary epithelial cells, we conducted quantitative real-time PCR (RT-qPCR)

assays. As shown in **Figure 6**, compared with normal breast cells (HS578BST), the expression of CENPF, TSPAN7, NEK2, TOP2A, COX7A1, SCN4B and ANLN were downregulated in tumor cell lines (MCF-7 and MDA-MB-231). Moreover, distinct expression patterns of the signature genes were observed across diverse breast cancer cell subtypes. MELK, BIRC5, UBE2T and KIF4A showed high expression level in MDA-MB-231, but with low expression in MCF-7. In contrast, GPIHBP1 exhibited an inverse expression pattern.

Preprint

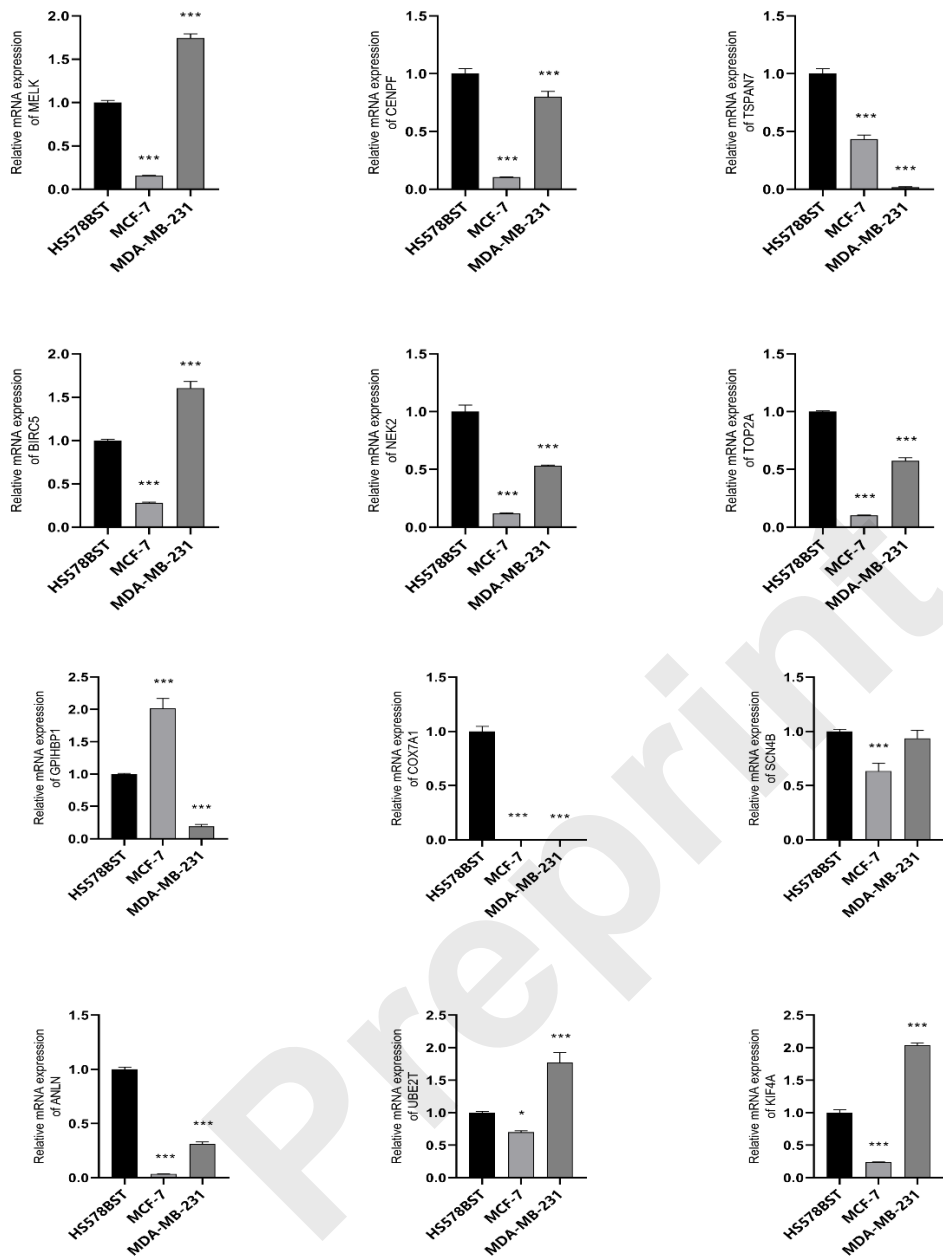


**Figure 6.** Validation of model genes in malignant and normal mammary epithelial cells.

#### 4.Discussion

tRNA acts as the "translator" of genetic information, uniquely recognizing mRNA codons through its anticodon and converting mRNA nucleotide sequences into peptide chains of nascent proteins. As research in transcriptomics advances, the roles of tRNA and mRNA in cancer are drawing increased attention[32]. Alterations in tRNA expression levels, structures, and functionalities can disrupt the translation of associated mRNAs[33, 34], influencing tumor development and prognosis. Therefore, tRNA and its related mRNA are crucial in the gene expression process within tumor cells[35, 36]. Although previous studies have identified tRNAs that influence the prognosis of BC, the impact of related mRNAs on the molecular mechanisms of BC has remained largely unexplored. In this study, we developed a model of tRNA-related mRNA that influences the prognosis of BC, demonstrating its potential value in predicting BC biological characteristics, immunotherapy responsiveness, and survival outcomes. Remarkably, our pan-cancer analysis has shown that this model is effective not only in predicting the prognosis of various other cancers but also in assessing the reactivity of the associated tumor microenvironment.

Beyond its canonical role in translational regulation, transfer RNA (tRNA) is increasingly recognized as a key modulator in diverse oncogenic processes, including the stabilization of mRNA, modulation of reverse transcription, and the regulation of apoptosis and cellular senescence[37]. During the senescence escape process of breast cancer cells, tRNA-Tyr is specifically upregulated and mediates the evasion of senescence through the mTOR pathway. Inhibiting mTOR can block this process[38]. In addition, tRNA can bind to RNA-binding proteins (such as YBX1) and regulate tumor cell metastasis and invasion[39]. We identified 5'-M-tRNA-Tyr-GTA-7-1\_L23 from the OncotRF database as an important prognostic marker for breast cancer (HR=1.265, p<0.001), which is significantly upregulated in breast cancer tissues[40]. Through bioinformatics analysis, we screened 12 characteristic genes from 92 closely related mRNAs and experimentally validated their differential expression between breast cancer and normal cells. Notably, MELK, BIRC5, GPIHBP1, UBE2T, and KIF4A were significantly upregulated in breast cancer cell lines; these genes have previously been implicated as potential therapeutic targets in breast cancer. The overexpression of these genes has been associated with unfavorable clinical outcomes in patients with breast cancer[41-45]. Given their coordinated upregulation with the tRNA, we hypothesize that this tRNA may facilitate tumor progression by interacting with the corresponding mRNAs and enhancing the translation of oncogenic transcripts. Nevertheless, the precise molecular mechanisms of the interaction between this tRNA and its mRNA targets remain to be elucidated, warranting further investigation.

We also constructed prognostic model based on the 12 characteristic genes and validated in both internal and external validation sets. This model accurately predicted BC patients' survival outcomes. To improve the clinical applicability of the model, we investigated the correlation between t-mRPM and clinical pathological features. Our findings indicate that this feature can help differentiate between T and M stages in BC patients. Based on this relationship, we constructed a nomogram to enhance the ability to predict overall survival rates. Analysis of the variations within HALLMARK pathways across different groups revealed that the high-risk group shows enrichment in biological processes and metabolic pathways associated with cancer. Additionally, there is a positive correlation seen between this risk score and the tumor's malignant characteristics, including angiogenesis, malignant proliferation, and the cell cycle. We investigated the relationship between t-mRPM and immunological traits in BC considering recent notable developments in the field of cancer immune microenvironment and immunotherapy [46-48]. The high-risk group exhibited reduced response to immunotherapy and a high infiltration of M2 macrophages, confirming the prognostic value of this risk model in the context of immunotherapy. Lastly, we performed a pan-cancer analysis to explore the possible use of this trait in additional tumor types. Our study shows that this characteristic has tremendous research potential as it not only predicts BC patients' prognosis accurately but also has a strong correlation with survival markers in other malignancies.

Currently, the use of Immune Checkpoint Inhibitors (ICIs) has revolutionized therapy for cancer patients[49-51]. The combination chemotherapy project comprising anti-PD-L1 atezolizumab and anti-PD-1 pembrolizumab has been approved as the first-line treatment for PD-L1 positive (PD-L1+) advanced Triple-Negative Breast Cancer (TNBC) patients[52]. Despite this, PD-L1 evaluation in tumor samples remains the sole biomarker currently guiding immunotherapeutic decisions in breast cancer. Unfortunately, many PD-L1+ tumor patients do not benefit from ICI treatments[53], highlighting the need for identifying and validating responsive biomarkers to optimize their therapeutic application. Our study suggests that t-mRNA associated with BC could serve as a potential biological predictor for the efficacy of ICI therapy, though further research is essential to validate this potential.

To our knowledge, this is the first study to construct a prognostic model for BC from the perspective of t-mRNA using machine learning, complemented by various pan-cancer analyses and RT-qPCR validation. However, we must acknowledge several limitations. Firstly, although we used multiple datasets to validate our model's predictive potential, most of the included cohorts are retrospective, and some datasets have small sample sizes. The application of this model's features needs further

validation in large-sample prospective studies and multicenter clinical trials. Secondly, our research relied on public databases. Future efforts should aim to confirm the specific mechanisms of these t-mRNA through additional cellular and tissue experimentation. In conclusion, the specific mechanisms and clinical application value of t-mRPM in cancer require further investigation and validation.

### **supplementary material**

The difference of biological functions in two risk groups and the research value of model genes in pan-cancer.

### **Acknowledgments**

None.

### **Author Contributions**

Conceptualization, Quan Yuan and Ming Niu; methodology, Quan Yuan; software, Rongjie Ye; validation, Rongjie Ye and Hao Yu; formal analysis, Quan Yuan; investigation, Ming Niu; data curation, Hao Yu; writing—original draft preparation, Quan Yuan and Rongjie Ye; writing—review and editing, Ming Niu and Ge Yu; visualization, Quan Yuan, Ming Niu and Ge Yu; supervision, Ming Niu and Ge Yu; project administration, Ge Yu; funding acquisition, Ming Niu and Ge Yu. All authors have read and agreed to the published version of the manuscript.

### **Conflict of interests**

The authors declare that they have no conflicts of interest.

### **Funding**

This work was supported by the Beijing Heart to Heart Foundation [grant numbers HXXT2021ktyj002, HXXT2021ktyj001]; Haiyan Science Foundation[grant numbers JJMS2022-08, JJZD2021-02].

### **Data availability statement**

The data underlying this article are available in the OncotRF database (<http://bioinformatics.zju.edu.cn/OncotRF>), the Gene Expression Omnibus (GEO) database (<https://www.ncbi.nlm.nih.gov/geo/>, [GSE20711](https://www.ncbi.nlm.nih.gov/geo/acc/show?acc=GSE20711) and [GSE20685](https://www.ncbi.nlm.nih.gov/geo/acc/show?acc=GSE20685)) and the Cancer Genome Atlas (TCGA) database (<https://tcga-data.nci.nih.gov/tcga/>).

## Reference

1. Li, H., et al., *Development and validation of a pathological model predicting the efficacy of neoadjuvant therapy for breast cancer based on RCB scoring*. Arch Med Sci, 2025. **21**(1): p. 92-101.
2. Siegel, R.L., A.N. Giaquinto, and A. Jemal, *Cancer statistics, 2024*. CA Cancer J Clin, 2024. **74**(1): p. 12-49.
3. Stabellini, N., et al., *Estimating the overall survival benefit of adjuvant chemo-endocrine therapy in women over age 50 with pT1-2N0 early stage breast cancer and 21-gene recurrence score  $\geq 26$ : A National Cancer Database analysis*. Cancer Med, 2023. **12**(19): p. 19607-19616.
4. Liu, C., et al., *Topical delivery of chemotherapeutic drugs using nano-hybrid hydrogels to inhibit post-surgical tumour recurrence*. Biomater Sci, 2021. **9**(12): p. 4356-4363.
5. Sambhi, M., et al., *Therapeutic Options for Metastatic Breast Cancer*. Adv Exp Med Biol, 2019. **1152**: p. 131-172.
6. Nunez, C., *Blood-based protein biomarkers in breast cancer*. Clin Chim Acta, 2019. **490**: p. 113-127.
7. Del Pilar Chantada-Vazquez, M., et al., *Proteomic investigation on bio-crown of Au, Ag and Fe nanoparticles for the discovery of triple negative breast cancer serum protein biomarkers*. J Proteomics, 2020. **212**: p. 103581.
8. Kumari, K., P. Groza, and F. Aguilo, *Regulatory roles of RNA modifications in breast cancer*. NAR Cancer, 2021. **3**(3): p. zcab036.
9. Guglas, K., et al., *Midsized noncoding RNAs in cancers: a new division that clarifies the world of noncoding RNA or an unnecessary chaos?* Rep Pract Oncol Radiother, 2022. **27**(6): p. 1077-1093.
10. Kovalski, J.R., D. Kuzuoglu-Ozturk, and D. Ruggero, *Protein synthesis control in cancer: selectivity and therapeutic targeting*. EMBO J, 2022. **41**(8): p. e109823.
11. Biela, A., et al., *The diverse structural modes of tRNA binding and recognition*. J Biol Chem, 2023. **299**(8): p. 104966.
12. Huang, Y., et al., *METTL1 promotes neuroblastoma development through m(7)G tRNA modification and selective oncogenic gene translation*. Biomark Res, 2022. **10**(1): p. 68.

13. Santos, M., et al., *Upregulation of tRNA-Ser-AGA-2-1 Promotes Malignant Behavior in Normal Bronchial Cells*. *Front Mol Biosci*, 2022. **9**: p. 809985.
14. Goodarzi, H., et al., *Modulated Expression of Specific tRNAs Drives Gene Expression and Cancer Progression*. *Cell*, 2016. **165**(6): p. 1416-1427.
15. Dedon, P.C. and T.J. Begley, *Dysfunctional tRNA reprogramming and codon-biased translation in cancer*. *Trends Mol Med*, 2022. **28**(11): p. 964-978.
16. Ma, J., et al., *METTL1/WDR4-mediated m(7)G tRNA modifications and m(7)G codon usage promote mRNA translation and lung cancer progression*. *Mol Ther*, 2021. **29**(12): p. 3422-3435.
17. Lyons, S.M., et al., *Identification of functional tetramolecular RNA G-quadruplexes derived from transfer RNAs*. *Nat Commun*, 2017. **8**(1): p. 1127.
18. Chen, H., et al., *Integrative analysis of PANoptosis-related genes in diabetic retinopathy: machine learning identification and experimental validation*. *Front Immunol*, 2024. **15**: p. 1486251.
19. Xu, C., et al., *Prediction of prognosis and survival of patients with gastric cancer by a weighted improved random forest model: an application of machine learning in medicine*. *Arch Med Sci*, 2022. **18**(5): p. 1208-1220.
20. Ye, R., et al., *Identification of the shared gene signatures in retinoblastoma and osteosarcoma by machine learning*. *Sci Rep*, 2024. **14**(1): p. 31355.
21. Cabrelle, C., F.M. Giorgi, and D. Mercatelli, *Quantitative and qualitative detection of tRNAs, tRNA halves and tRFs in human cancer samples: Molecular grounds for biomarker development and clinical perspectives*. *Gene*, 2024. **898**: p. 148097.
22. Kwon, N.H., J.Y. Lee, and S. Kim, *Role of tRNAs in Breast Cancer Regulation*. *Adv Exp Med Biol*, 2021. **1187**: p. 121-145.
23. Otasek, D., et al., *Cytoscape Automation: empowering workflow-based network analysis*. *Genome Biol*, 2019. **20**(1): p. 185.
24. Yuan, Y., et al., *Circulating exosome long non-coding RNAs are associated with atrial structural remodeling by increasing systemic inflammation in atrial fibrillation patients*. *J Transl Int Med*, 2024. **12**(1): p. 106-118.
25. Degenhardt, F., S. Seifert, and S. Szymczak, *Evaluation of variable selection methods for random forests and omics data sets*. *Brief Bioinform*, 2019. **20**(2): p. 492-503.

26. Liu, S., et al., *Three Differential Expression Analysis Methods for RNA Sequencing: limma, EdgeR, DESeq2*. J Vis Exp, 2021(175).
27. Hanzelmann, S., R. Castelo, and J. Guinney, *GSEA: gene set variation analysis for microarray and RNA-seq data*. BMC Bioinformatics, 2013. **14**: p. 7.
28. Wu, T., et al., *clusterProfiler 4.0: A universal enrichment tool for interpreting omics data*. Innovation (Camb), 2021. **2**(3): p. 100141.
29. Zhang, Z., L. Zhang, and Y. Shen, *Identification of immune features of HIV-infected patients with antiretroviral therapy through bioinformatics analysis*. Virology, 2022. **566**: p. 69–74.
30. Zhong, X., et al., *Cellular components in tumor microenvironment of neuroblastoma and the prognostic value*. PeerJ, 2019. **7**: p. e8017.
31. Henriques, B., F. Mendes, and D. Martins, *Immunotherapy in Breast Cancer: When, How, and What Challenges?* Biomedicines, 2021. **9**(11).
32. Wang, L. and S. Lin, *Emerging functions of tRNA modifications in mRNA translation and diseases*. J Genet Genomics, 2023. **50**(4): p. 223–232.
33. Zhang, R., et al., *The biological process of lysine-tRNA charging is therapeutically targetable in liver cancer*. Liver Int, 2021. **41**(1): p. 206–219.
34. Li, P., et al., *The m(5) C methyltransferase NSUN2 promotes codon-dependent oncogenic translation by stabilising tRNA in anaplastic thyroid cancer*. Clin Transl Med, 2023. **13**(11): p. e1466.
35. Wang, Y., et al., *tRNA modifications: insights into their role in human cancers*. Trends Cell Biol, 2023. **33**(12): p. 1035–1048.
36. Kochavi, A., et al., *Proteome diversification by mRNA translation in cancer*. Mol Cell, 2023. **83**(3): p. 469–480.
37. Pekarsky, Y., V. Balatti, and C.M. Croce, *tRNA-derived fragments (tRFs) in cancer*. J Cell Commun Signal, 2023. **17**(1): p. 47–54.
38. Guillon, J., et al., *tRNA biogenesis and specific aminoacyl-tRNA synthetases regulate senescence stability under the control of mTOR*. PLoS Genet, 2021. **17**(12): p. e1009953.
39. Goodarzi, H., et al., *Endogenous tRNA-Derived Fragments Suppress Breast Cancer Progression via YBX1 Displacement*. Cell, 2015. **161**(4): p. 790–802.

40. Pavon-Eternod, M., et al., *tRNA over-expression in breast cancer and functional consequences*. Nucleic Acids Res, 2009. **37**(21): p. 7268–80.
41. Das, A., et al., *Structure-based virtual screening of chemical libraries as potential MELK inhibitors and their therapeutic evaluation against breast cancer*. Chem Biol Interact, 2023. **376**: p. 110443.
42. Al-Yahya, S., et al., *Post-transcriptional regulation of BIRC5/survivin expression and induction of apoptosis in breast cancer cells by tristetraprolin*. RNA Biol, 2024. **21**(1): p. 1–15.
43. Bao, Y., et al., *Transcriptome profiling revealed multiple genes and ECM-receptor interaction pathways that may be associated with breast cancer*. Cell Mol Biol Lett, 2019. **24**: p. 38.
44. Wang, K., et al., *Targeting UBE2T suppresses breast cancer stemness through CBX6-mediated transcriptional repression of SOX2 and NANOG*. Cancer Lett, 2024. **611**: p. 217409.
45. Yang, K., et al., *MiR-379-5p inhibits the proliferation, migration, and invasion of breast cancer by targeting KIF4A*. Thorac Cancer, 2022. **13**(13): p. 1916–1924.
46. He, J.J., et al., *Advancement and Applications of Nanotherapy for Cancer Immune Microenvironment*. Curr Med Sci, 2023. **43**(4): p. 631–646.
47. Huber, M., et al., *The Immune Microenvironment in Pancreatic Cancer*. Int J Mol Sci, 2020. **21**(19).
48. Liu, F., et al., *Methylation of FAM110C is a synthetic lethal marker for ATR/CHK1 inhibitors in pancreatic cancer*. J Transl Int Med, 2024. **12**(3): p. 274–287.
49. Wang, Y., et al., *New developments in the mechanism and application of immune checkpoint inhibitors in cancer therapy (Review)*. Int J Oncol, 2023. **63**(1).
50. Wu, Y.X., et al., *Application of immune checkpoint inhibitors in immunotherapy for gastric cancer*. Immunotherapy, 2023. **15**(2): p. 101–115.
51. Deng, X., *A case of vaginal melanoma with multi-line immunotherapy and reflections*. Arch Med Sci, 2023. **19**(6): p. 1923–1928.
52. Wu, J., et al., *Global research trends on anti-PD-1/anti-PD-L1 immunotherapy for triple-negative breast cancer: A scientometric analysis*. Front Oncol, 2022. **12**: p. 1002667.

53. Liu, Q., et al., *Molecular and Clinical Characterization of PD-1 in Breast Cancer Using Large-Scale Transcriptome Data*. *Front Immunol*, 2020. **11**: p. 558757.

Preprint

UCSC Xana  
GEO  
GSE20811 GSE20754  
OncotRF Database

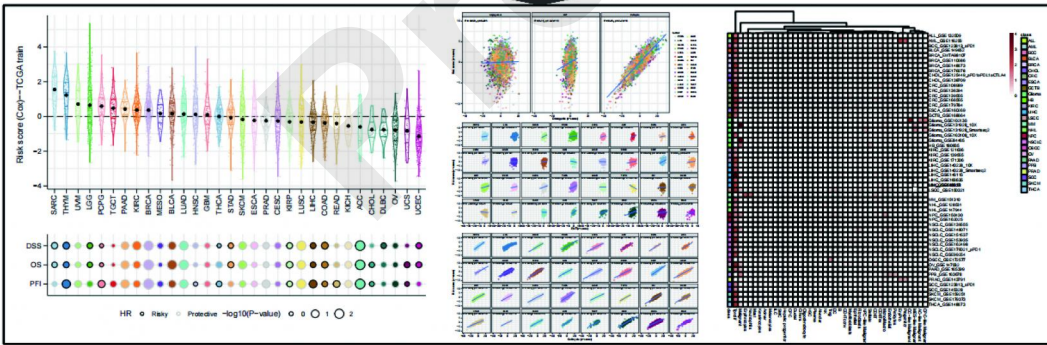
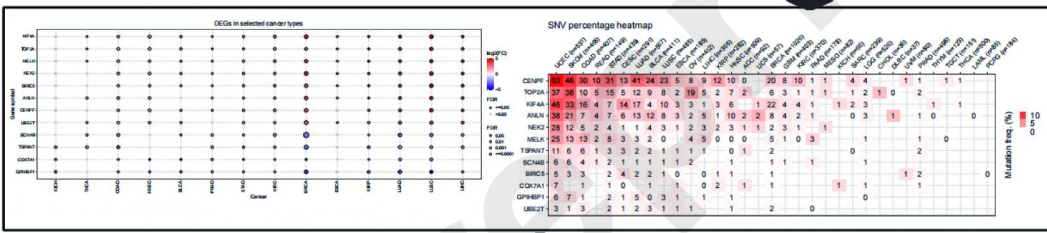
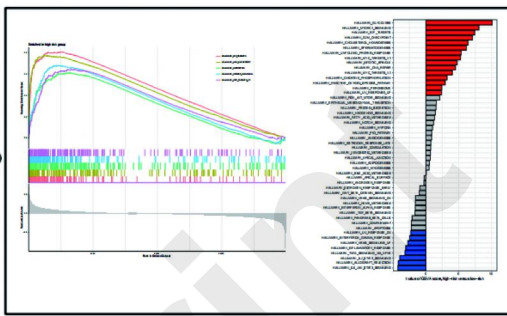
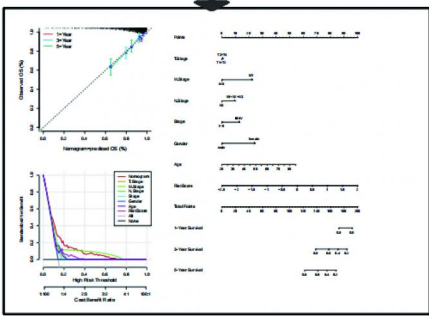
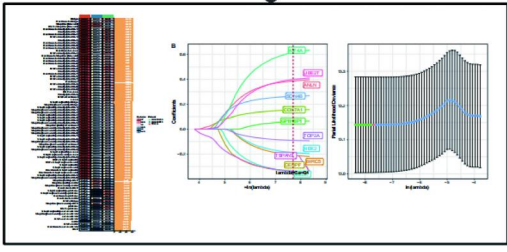
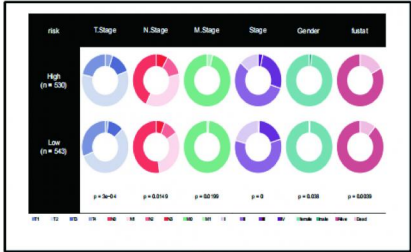
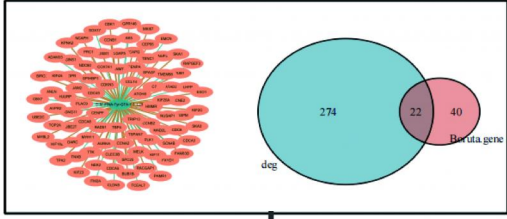
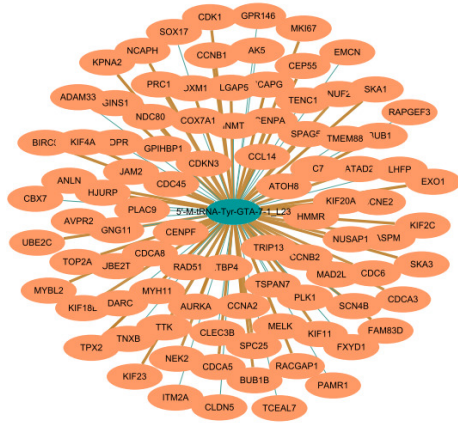


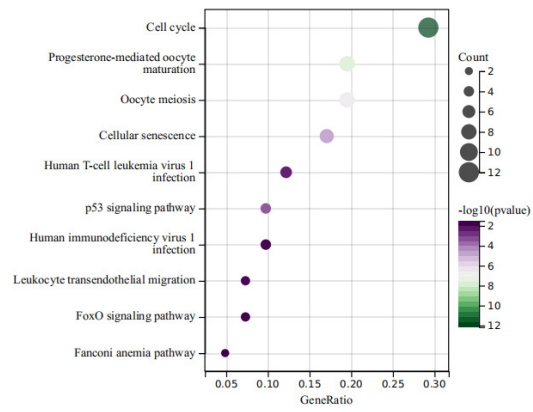
**Table 1. RT-qPCR primer sequences used in the study.**

| Primer name     | Primer sequence ( 5'→3') |
|-----------------|--------------------------|
| h-MELK-169-F    | TATTCACCTCGATGATGATTGCG  |
| h-MELK-169-R    | AGAAAGCCTTAAACGAACTGGTT  |
| h-CENPF-102-F   | CTCTCCCGTCAACAGCGTTC     |
| h-CENPF-102-R   | GTTGTGCATATTCTTGGCTTGC   |
| h-TSPAN7-242-F  | TATCTCCCTTATTGCCGAGAACT  |
| h-TSPAN7-242-R  | TAGCGTCCGTGTAAGTCCTCA    |
| h-BIRC5-118-F   | AGGACCACCGCATCTCTACAT    |
| h-BIRC5-118-R   | AAGTCTGGCTCGTTCTCAGTG    |
| h-NEK2-233-F    | CTGGATGGCAAGCAAAACGTC    |
| h-NEK2-233-R    | CCAGCGAGTTCTTTCTGGCTA    |
| h-TOP2A-129-F   | ACCATTGCAGCCTGTAAATGA    |
| h-TOP2A-129-R   | GGGCGGAGCAAAATATGTTCC    |
| h-GPIHBP1-194-F | GCAACCTGACGCAGAACTG      |
| h-GPIHBP1-194-R | CCAGGGTGGGACATTGCAC      |
| h-COX7A1-132-F  | GAGTGCGCGAGAAACAGAAG     |
| h-COX7A1-132-R  | ACAAGCTGTAGACAGTGCCG     |
| h-SCN4B-179-F   | CTGGGCTTTTGGTGGAAGAAG    |
| h-SCN4B-179-R   | GTTGTCATTCCCCGAGGAGC     |
| h-ANLN-130-F    | TGGAGAAGAGCCAAGAGGAG     |
| h-ANLN-130-R    | TCTGGACTTACCACACCAACTG   |
| h-UBE2T-226-F   | AGCTGCTCATGTCAGAACCC     |
| h-UBE2T-226-R   | ACTAGCTGACTGGCCTTCCT     |
| h-KIF4A-139-F   | ACGCCATCTGAATGACCTCC     |
| h-KIF4A-139-R   | ACCACGCACTTCAGTAAGGG     |
| hGAPDH-172-F    | CTGACTTCAACAGCGACACC     |
| hGAPDH-172-R    | GTGGTCCAGGGGTCTTACTC     |

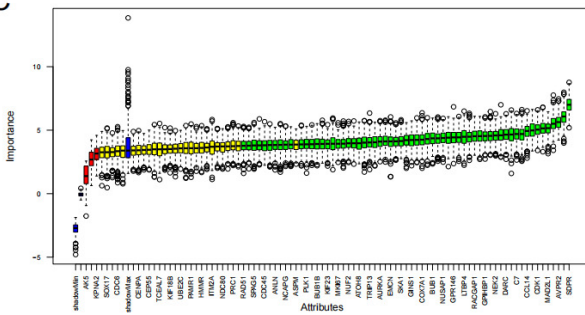
A



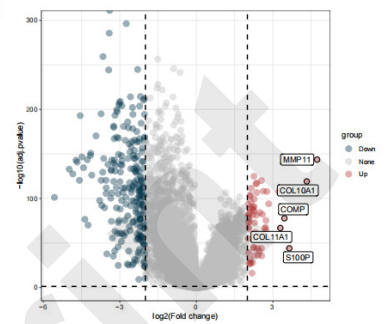
B



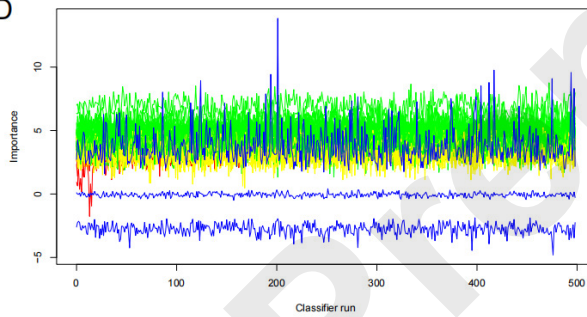
C



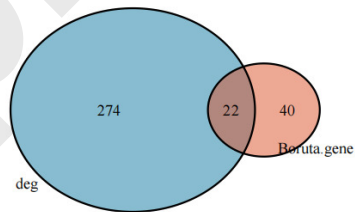
E



D



F

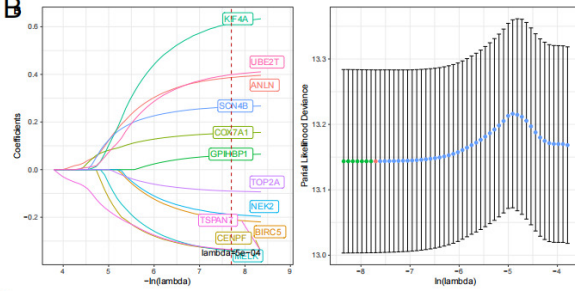


Identification of DET-mRNA.

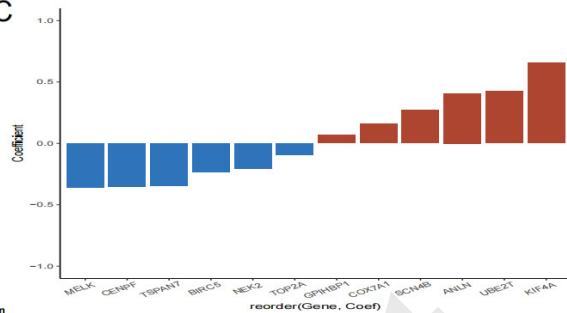
A

|                                   |       |       |       |       |
|-----------------------------------|-------|-------|-------|-------|
| Ridge                             | 0.652 | 0.592 | 0.604 | 0.616 |
| CoxBoost+Ridge                    | 0.656 | 0.576 | 0.610 | 0.615 |
| StepCox[forward]                  | 0.659 | 0.629 | 0.556 | 0.615 |
| RSF+StepCox[forward]              | 0.659 | 0.629 | 0.556 | 0.615 |
| CoxBoost+enet(alpha=0.1)          | 0.659 | 0.574 | 0.607 | 0.613 |
| enet(alpha=0.1)                   | 0.655 | 0.574 | 0.611 | 0.613 |
| CoxBoost+enet(alpha=0.2)          | 0.660 | 0.575 | 0.602 | 0.612 |
| RSF+enet(alpha=0.1)               | 0.653 | 0.564 | 0.617 | 0.611 |
| enet(alpha=0.2)                   | 0.655 | 0.568 | 0.612 | 0.611 |
| CoxBoost+enet(alpha=0.5)          | 0.661 | 0.577 | 0.596 | 0.611 |
| CoxBoost+enet(alpha=0.8)          | 0.661 | 0.578 | 0.594 | 0.611 |
| CoxBoost+enet(alpha=0.3)          | 0.659 | 0.571 | 0.602 | 0.611 |
| CoxBoost+Lasso                    | 0.661 | 0.577 | 0.594 | 0.611 |
| RSF+enet(alpha=0.2)               | 0.652 | 0.563 | 0.616 | 0.611 |
| CoxBoost+StepCox[forward]         | 0.662 | 0.575 | 0.594 | 0.611 |
| CoxBoost+enet(alpha=0.4)          | 0.660 | 0.574 | 0.597 | 0.61  |
| CoxBoost+enet(alpha=0.9)          | 0.661 | 0.575 | 0.595 | 0.61  |
| CoxBoost+enet(alpha=0.6)          | 0.660 | 0.575 | 0.596 | 0.61  |
| enet(alpha=0.4)                   | 0.653 | 0.568 | 0.610 | 0.61  |
| RSF+enet(alpha=0.3)               | 0.649 | 0.565 | 0.616 | 0.61  |
| enet(alpha=0.5)                   | 0.649 | 0.568 | 0.612 | 0.609 |
| CoxBoost+enet(alpha=0.7)          | 0.659 | 0.570 | 0.598 | 0.609 |
| RSF+enet(alpha=0.5)               | 0.651 | 0.566 | 0.609 | 0.609 |
| RSF+enet(alpha=0.7)               | 0.654 | 0.568 | 0.604 | 0.609 |
| CoxBoost                          | 0.654 | 0.568 | 0.603 | 0.608 |
| RSF+enet(alpha=0.9)               | 0.649 | 0.565 | 0.606 | 0.608 |
| enet(alpha=0.6)                   | 0.652 | 0.564 | 0.607 | 0.608 |
| RSF+enet(alpha=0.6)               | 0.656 | 0.563 | 0.603 | 0.608 |
| RSF+Lasso                         | 0.653 | 0.566 | 0.602 | 0.607 |
| enet(alpha=0.9)                   | 0.655 | 0.565 | 0.601 | 0.607 |
| RSF+CoxBoost                      | 0.656 | 0.563 | 0.600 | 0.606 |
| Lasso                             | 0.654 | 0.563 | 0.601 | 0.606 |
| StepCox[both]+Ridge               | 0.653 | 0.560 | 0.590 | 0.601 |
| StepCox[backward]+Ridge           | 0.654 | 0.558 | 0.585 | 0.599 |
| StepCox[both]+enet(alpha=0.1)     | 0.655 | 0.556 | 0.582 | 0.598 |
| StepCox[backward]+enet(alpha=0.1) | 0.655 | 0.553 | 0.580 | 0.596 |
| StepCox[backward]+enet(alpha=0.2) | 0.655 | 0.553 | 0.581 | 0.596 |
| StepCox[both]+enet(alpha=0.2)     | 0.655 | 0.554 | 0.579 | 0.596 |
| StepCox[both]+enet(alpha=0.3)     | 0.656 | 0.553 | 0.578 | 0.596 |
| StepCox[both]+enet(alpha=0.4)     | 0.656 | 0.553 | 0.578 | 0.595 |
| StepCox[backward]+enet(alpha=0.5) | 0.656 | 0.552 | 0.578 | 0.595 |
| StepCox[backward]+enet(alpha=0.3) | 0.656 | 0.552 | 0.577 | 0.595 |
| StepCox[backward]+enet(alpha=0.8) | 0.656 | 0.554 | 0.575 | 0.595 |
| StepCox[both]+enet(alpha=0.7)     | 0.656 | 0.554 | 0.575 | 0.595 |
| StepCox[both]+enet(alpha=0.6)     | 0.656 | 0.553 | 0.575 | 0.595 |
| StepCox[backward]+enet(alpha=0.4) | 0.656 | 0.552 | 0.576 | 0.595 |
| StepCox[backward]+CoxBoost        | 0.656 | 0.553 | 0.578 | 0.595 |
| StepCox[both]+enet(alpha=0.9)     | 0.656 | 0.554 | 0.573 | 0.594 |
| StepCox[backward]+enet(alpha=0.9) | 0.656 | 0.554 | 0.573 | 0.594 |
| StepCox[both]+Lasso               | 0.656 | 0.554 | 0.573 | 0.594 |
| StepCox[backward]+Lasso           | 0.656 | 0.554 | 0.573 | 0.594 |
| StepCox[both]+enet(alpha=0.8)     | 0.656 | 0.554 | 0.573 | 0.594 |
| RSF+StepCox[both]                 | 0.656 | 0.554 | 0.572 | 0.594 |
| RSF+StepCox[backward]             | 0.656 | 0.554 | 0.572 | 0.594 |
| StepCox[both]                     | 0.656 | 0.554 | 0.572 | 0.594 |
| StepCox[backward]                 | 0.656 | 0.554 | 0.572 | 0.594 |
| CoxBoost+StepCox[both]            | 0.656 | 0.554 | 0.572 | 0.594 |
| CoxBoost+StepCox[backward]        | 0.656 | 0.554 | 0.572 | 0.594 |
| StepCox[both]+enet(alpha=0.5)     | 0.656 | 0.553 | 0.573 | 0.594 |
| StepCox[backward]+enet(alpha=0.6) | 0.656 | 0.553 | 0.573 | 0.594 |
| StepCox[both]+RSF                 | 0.560 | 0.621 | 0.530 | 0.57  |
| StepCox[both]+GBM                 | 0.563 | 0.607 | 0.533 | 0.568 |
| StepCox[backward]+GBM             | 0.560 | 0.603 | 0.528 | 0.564 |
| CoxBoost+RSF                      | 0.564 | 0.596 | 0.524 | 0.561 |
| StepCox[both]+plsRcox             | 0.572 | 0.495 | 0.622 | 0.569 |
| StepCox[backward]+plsRcox         | 0.572 | 0.495 | 0.622 | 0.569 |
| CoxBoost+plsRcox                  | 0.567 | 0.495 | 0.617 | 0.567 |
| CoxBoost+GBM                      | 0.558 | 0.583 | 0.526 | 0.558 |
| RSF+Ridge                         | 0.556 | 0.495 | 0.615 | 0.556 |
| StepCox[backward]+RSF             | 0.534 | 0.603 | 0.525 | 0.554 |
| plsRcox                           | 0.552 | 0.495 | 0.612 | 0.553 |
| RSF+plsRcox                       | 0.552 | 0.495 | 0.612 | 0.553 |
| StepCox[both]+survivalSVM         | 0.545 | 0.538 | 0.562 | 0.548 |
| StepCox[backward]+survivalSVM     | 0.545 | 0.538 | 0.562 | 0.548 |
| survivalSVM                       | 0.530 | 0.529 | 0.576 | 0.545 |
| RSF+survivalSVM                   | 0.530 | 0.529 | 0.576 | 0.545 |
| GBM                               | 0.544 | 0.567 | 0.564 | 0.538 |
| RSF+GBM                           | 0.555 | 0.536 | 0.526 | 0.532 |
| CoxBoost+survivalSVM              | 0.514 | 0.538 | 0.541 | 0.531 |
| RSF                               | 0.545 | 0.468 | 0.536 | 0.523 |

B



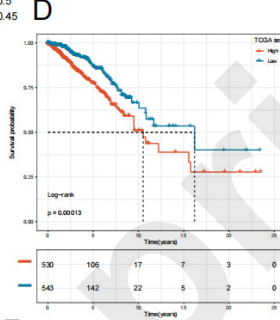
C



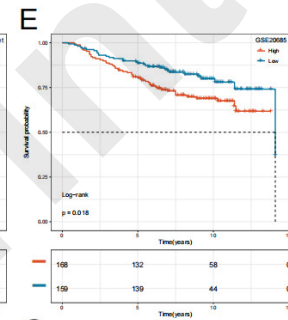
C-in



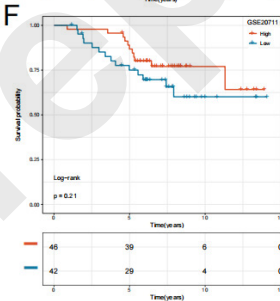
D



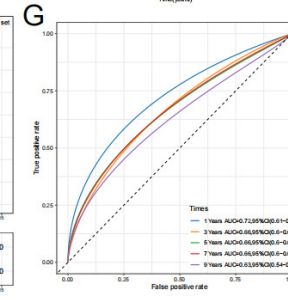
E



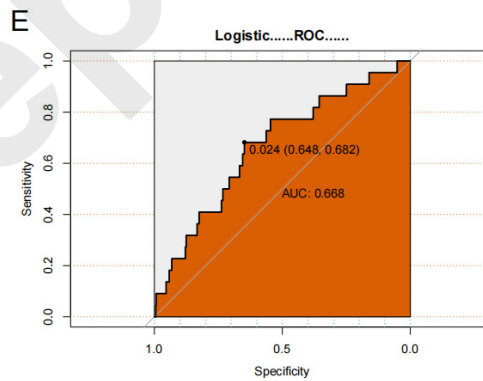
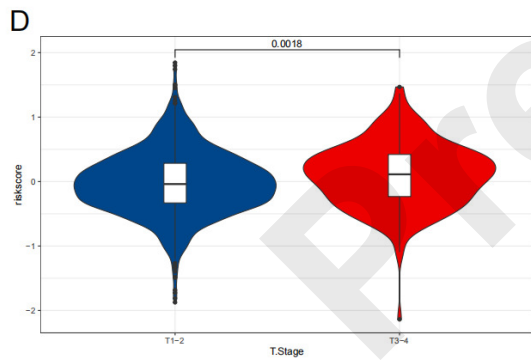
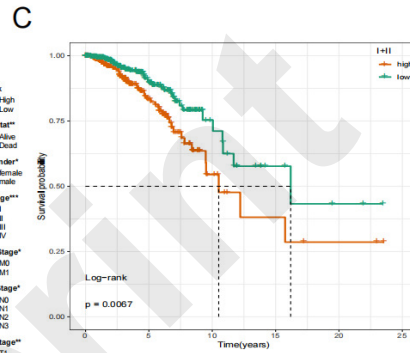
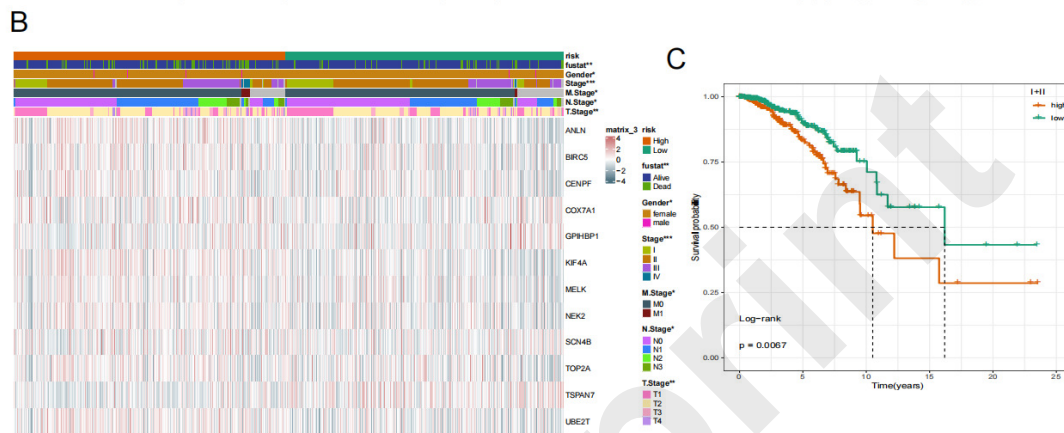
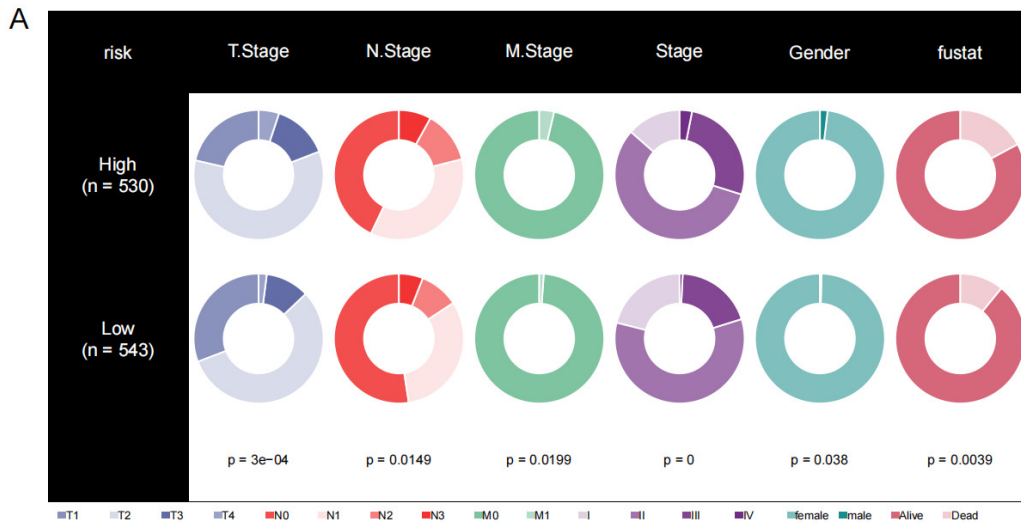
F



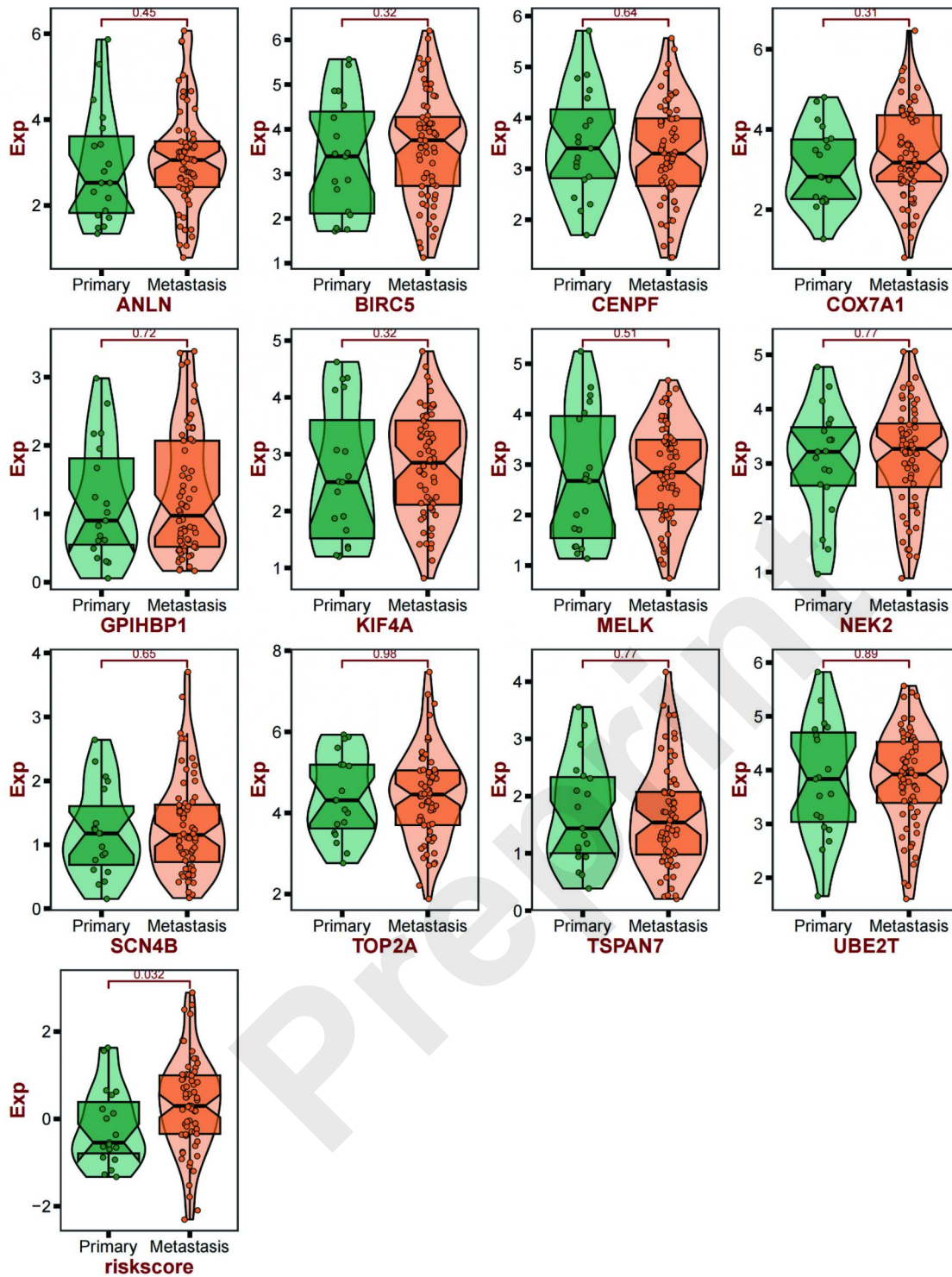
G



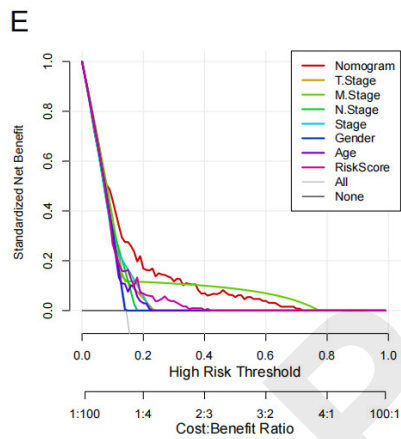
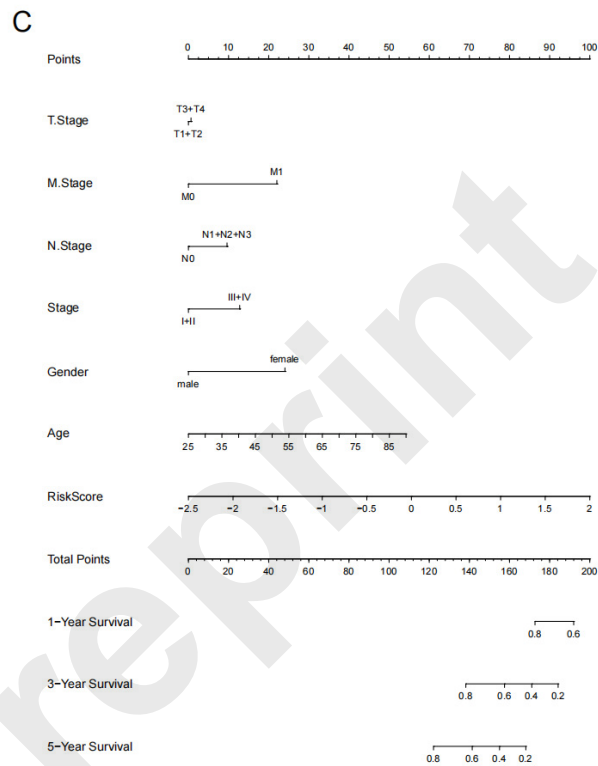
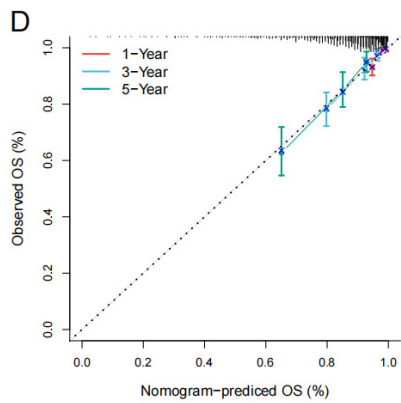
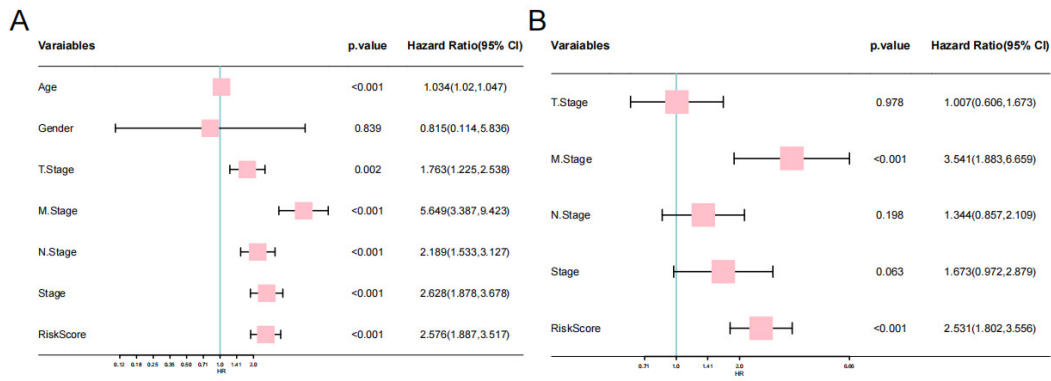
Construction and validation of t-mRPM.



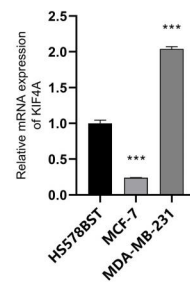
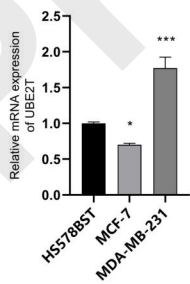
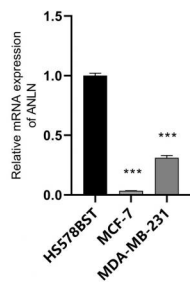
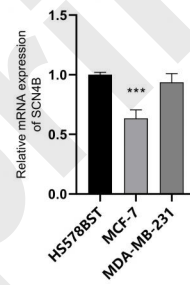
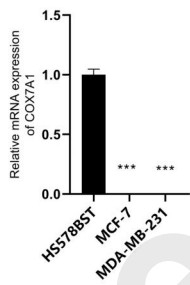
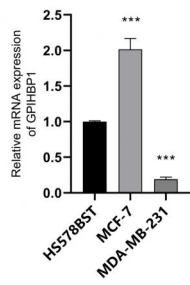
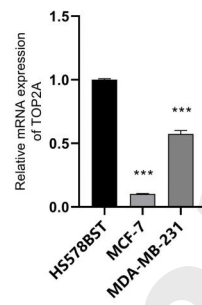
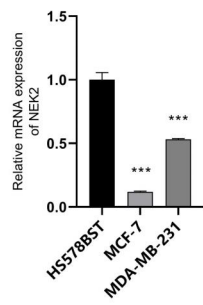
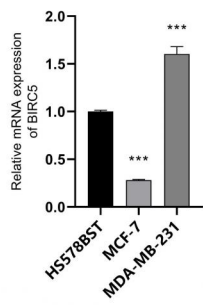
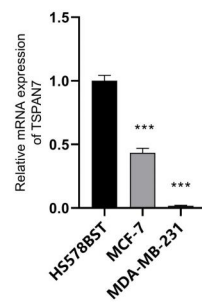
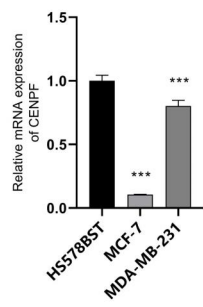
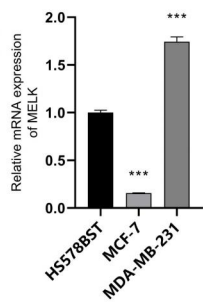
Analysis of correlations between clinicopathological features and the prognostic model in the TCGA cohort.



Expression levels of individual model genes in the BC metastasis cohort.



Analysis of the clinical pathological characteristics of t-mRPM and its independent prognostic potential.



Validation of model genes in malignant and normal mammary epithelial cells.